JACS
JOURNAL OF THE AMERICAN CHEMICAL SOCIETY
Article
pubs.acs.org/JACS

Single-Molecule Patch-Clamp FRET Anisotropy Microscopy Studies of NMDA Receptor Ion Channel Activation and Deactivation under Agonist Ligand Binding in Living Cells

Dibyendu Kumar Sasmal, Rajeev Yadav, and H. Peter Lu*

Center for Photochemical Sciences, Department of Chemistry, Bowling Green State University, Bowling Green, Ohio 43403, United States

ABSTRACT: *N*-methyl-D-aspartate (NMDA) receptor ion channel is activated by the binding of two pairs of glycine and glutamate along with the application of action potential. Binding and unbinding of ligands changes its conformation that plays a critical role in the open−close activities of NMDA receptor. Conformation states and their dynamics due to ligand binding are extremely difficult to characterize either by conventional ensemble experiments or single-channel electrophysiology method. Here we report the development of a new correlated technical approach, single-molecule patch-clamp FRET anisotropy imaging and demonstrate by probing the dynamics of NMDA receptor ion channel and kinetics of glycine binding with its ligand binding domain. Experimentally determined kinetics of ligand binding with receptor is further verified by computational modeling. Single-channel patch-clamp and four-channel fluorescence measurement are recorded simultaneously to get correlation among electrical on and off states, optically determined conformational open and closed states by FRET, and binding-unbinding states of the glycine ligand by anisotropy measurement at the ligand binding domain of GluN1 subunit. This method has the ability to detect the intermediate states in addition to electrical on and off states. Based on our experimental results, we have proposed that NMDA receptor gating goes through at least one electrically intermediate off state, a desensitized state, when ligands remain bound at the ligand binding domain with the conformation similar to the fully open state.

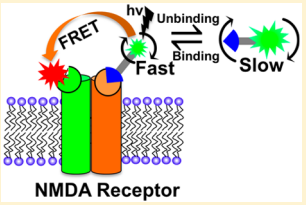

1. INTRODUCTION

N-methyl-D-aspartate (NMDA) receptor is a crucial ion channel membrane protein among the ligand-gated ion channels at the neuronal synapses, important for controlling synaptic plasticity and memory functions.[1] Furthermore, NMDA receptor ion channel is unique because it requires binding of both agonists, glycine and glutamate, for activation, and membrane depolarization to unblock magnesium (Mg^{2+}) ion from the transmembrane domain (TMD).[2−35] The prerequisite for simultaneous chemical and electrical stimuli, and the subsequent activation resulting with influx of calcium (Ca^{2+}) and potassium ion (K^{+}) through the TMD, distinguishes the NMDA receptor from other glutamate receptors, e.g., AMPA and kainate ionotropic glutamate receptors.[2,9,16] The crystal structure of intact NMDA receptor is recently reported at an unprecedented detail with resolution of 4 Å.[9,16] This is a heterotetramer consisting of two GluN1 and two GluN2 subunits and is activated upon concurrent binding of glycine and glutamate to the ligand binding domain (LBD) of GluN1 and GluN2 subunits, respectively, which then release the magnesium ion block from the pore of the ion channel by membrane depolarization. The NMDA receptors are arranged as a dimer of GluN1-GluN2 heterodimers with the two-fold symmetry axis (C_2) with respect to subunits, and each subunit is composed of an amino terminal domain (ATD), a LBD, and a TMD. The ATD and LBD are much more highly packed in the NMDA receptors compared to non-NMDA receptors that may explain the involvement of ATD in the ion channel activity of NMDA receptors. The overall structure of NMDA receptor bound to glycine and glutamate is like a hot-air balloon bound to a basket, where balloon and basket correspond to the extracellular domains and TMD, respectively. The TMD with tetrameric subunits has a pseudo-four-fold symmetry, except for the tilt angle of the M4 helix in GluN2B. The tetrameric crossing of M3 makes the pathway of ion penetration through TMD. The tunnel pore of the NMDA receptor ion channel shows high structural similarity with the crystal structure of the potassium ion channel despite sequence similarity.[16] Having structural similarity with the potassium channel, it is speculated that the gating NMDA receptor, composed of GluN1a and GluN2B subunits, may involve rearrangement of M3 helices.[16] Compared to the potassium ion channel, one of the main functions of the NMDA receptor is to control the permeability of Ca^{2+} ion through it.[2,5,18−20,35] The influx of Ca^{2+} ions in the cell due to opening of NMDA receptor triggers the signal transduction cascade, which controls the strength of neural connectivity or neuroplasticity. Hyper- or hypo-activation of NMDA receptors is entailed in neurological disorders and diseases including depression, schizophrenia, Parkinson's disease, Alzheimer's disease, and ischemic injuries associated with stroke.[2] However, recent advancements of structure based on the understanding of selective ion permeability and blocking of transmembrane by Mg^{2+} still need to be addressed.

Received: April 5, 2016
Published: June 7, 2016

DOI: 10.1021/jacs.6b03496
J. Am. Chem. Soc. 2016, 138, 8789−8801

To understand the relation between structure and function of NMDA receptor ion channel, different types of experimental techniques,[2−23,25−30,32−35] e.g., X-ray crystallography and electrophysiology as well as molecular dynamics simulation, have been applied.[24,31] Zhou and co-workers have developed an atomistic simulation model to study subunit specific contribution to the gating mechanism of NMDA receptor by targeted molecular dynamics simulation. They have shown that the lobe closure to the LBD produces an upward pulling upon binding with agonist.[23,30] The upward pulling of C-terminal induce a translational motion in LBD, which results to the opening of ion channel. This pulling force is more for a GluN2 subunit than a GluN1 subunit, and thus a GluN2 subunit contributes more in NMDA receptor channel gating. With this simulation model, they also predict that the Ca^{2+} cations are attracted toward the mouth of the ion channel pore via a strong negative electrostatic potential and the ion enters into the channel pore and thereafter solvated.[23,30] The structure of isolated LBD monomer bound to agonist and antagonist has been reported previously.[12,14] Those structures reveal that the clamshell of LBD is open when it is bound with antagonists and closed when bound with agonists molecules. The structure of dimer of GluN1 and GluN2 bound to glycine and glutamate has also been reported previously.[13,14] To understand the structure−function relation and dynamics of NMDA receptor, it is necessary to view the protein structure at the condition of some functions, such as membrane potential, ligand-induced channel gating, Ca^{2+}/Na^{+} ion permeability, interdomain interaction, etc. Very recently, a detailed view of intact heterotetrameric NMDA receptor ion channel composed of ATD, LBD, and TMD has been reported by high-resolution X-ray crystallography.[9] It is reported that interdomain interaction between LBD and ATD plays a key role in the function of the NMDA receptor ion channel. The ATD and LBD are tightly packed to each other compared to the AMPA receptor, and thus ATD also plays a crucial role in the functioning of the NMDA receptor ion channel. Recently, Gouaux and co-workers have reported the unprecedented 3D view of extracellular domains and TMD of the NMDA receptor by X-ray crystallography in the presence of ion channel blocker, partial agonist, and inhibitor and showed that the TMD has a structural similarity with the voltage gated potassium channel, and thus gating of NMDA receptor may involve M3 helicies.[9] They have also shown that the close packed structure between ATD and LBD plays a crucial role in ion channel gating mechanism. The extracellular ends of the M3 helicies of TMD form a pyramid-like shape, and it may explain the Mg^{2+} blocking and Ca^{2+} permeability through the TMD.[9]

Correlated optical and current measurement is becoming increasingly popular to understand structure−function relationship of an ion channel in detail because the information received by the simultaneous measurement creates a true molecular movie which is never be visible in either single-channel or optical measurement.[37−68] In 1999, Yanagida and co-workers first studied the activity of a single ion channel in an artificial lipid bilayer using simultaneous measurements of electric current and spectroscopic parameters.[67] Patch-clamp is an important tool primarily because it provides a direct measure of an ion channel's function. Measuring ionic flux provides a relatively easy way of probing protein function in comparison to other classes of membrane protein. However, probing channel function is only one-half of the picture. Along with the functioning of a protein and ion channel, it becomes important to probe the conformational intermediate states for understanding the complete scenario of structure and function relationship of the protein and ion channel.[69−76] Warshel and co-workers have performed molecular dynamic simulations to understand the detailed mechanism of the activation of voltage gated ion channel, Kv1.2, and examined the energetics of observed intermediate states along with open and closed states of ion channel.[75] To relate channel function to an actual mechanism of gating and structural changes happening within the channel, it is also required to understand by other methods, e.g., single-molecule FRET, which is a powerful and sensitive approach for probing the conformational intermediate states of proteins and ion channel receptors.[32,37,38,41,52,56,59,60,77−80] For example, Ha and Nichols have examined the structural dynamics of potassium channel, KirBac1.1 within lipid membrane using single-molecule FRET.[81] There are a number of reports that used single-molecule imaging and super-resolution imaging for the neuronal activity as well as dynamics, tracking of receptors in the chemical synapse of the live cell.[82−85] However, single-channel recording predates single-molecule fluorescence methods. The reason is straightforward: single-channel conductance can measure 10^8 ions per second in real time, whereas maximum photon emission rates for a single fluorophore is around 10^5 photons per second per molecule.[37,59] Again, the maximum photon detection ability of a microscope setup is 10−15% of the number of photons emitted by a fluorophore. So, it is technically easier to detect ions than photons. Single channel electric recording data can only detect and interpret fully on and off state of an ion channel. Single-molecule FRET can detect the conformational open and closed states of an ion channel by measuring the distance between the subunits. For example, Lu and co-workers have reported the existence of multiple intermediate states of gramicidin ion channel in artificial membranes by single-molecule patch-clamp fluorescence microscopy.[59] They have also interpreted observations in case of NMDA receptor in living cell by patch-clamp FRET microscopy.[32] Two electric on and off states are associated with multiple intermediate conformational closed states, which are identified by single-molecule fluorescence spectroscopic imaging at the electric off states of the ion channels.

In this article, we demonstrate a new technical approach, single-molecule patch-clamp FRET anisotropy imaging studies of NMDA receptor ion channel dynamics in HEK-293 cells. Applying this combined approach, we are able to record single-channel patch-clamp and four-channel fluorescence measurement simultaneously to get correlation of electrically on and off states by patch-clamp electric recording, optically determined conformational closed and open states by FRET, and binding−unbinding states of glycine ligand by anisotropy measurement at the LBD of GluN1 subunit. The single-channel electric on−off trajectories have been correlated in real-time with simultaneous changes in single-molecule FRET trajectories and single-molecule anisotropy trajectories to probe ion-channel open−close conformational dynamics and binding−unbinding state of ligand, respectively. Our results further characterized the occurrence of close intermediate conformational states bound to ligand that are associated with similar electric off states of the NMDA receptor ion channels. The ligand bound closed states are called desensitized states. The agonist binding kinetics determined by the new technique is further verified by computational modeling. Our experimental and computational results reveal the complex relationship of

DOI: 10.1021/jacs.6b03496
J. Am. Chem. Soc. 2016, 138, 8789−8801

the fluctuating structure, function and conformational changes as a consequence of binding of ligand. This dynamic structure−function relationship cannot be determined by any conventional experimental methods (e.g., X-ray crystallography). Finally, the free energy of binding of agonist with receptor observed from theoretical calculations is compared with the experimental results.

2. MATERIALS AND EXPERIMENTAL SECTION

Chemicals are purchased from Sigma, Invitrogen, and ATCC for single-molecule patch-clamp FRET anisotropy experiments. They are used for experiments without further purification.

2.1. Cell Culture, Plasmid Amplification, and Heterogeneous Expression of NMDA Receptor Ion Channel in HEK-293 Cell. HEK-293 cells are cultured in 75 cm^2 flask in EMEM (ATCC, 30−2003) supplemented with 10% fetal bovine serum (ATCC, 30-2020) and 1% penicillin-streptomycin (Gibco, 15070-063) at 37 °C in a 5% CO_2 atmosphere. After 2−3 days, cells are subcultured when they reached ∼75% confluence on the surface of 75 cm^2 flask. For live cell imaging and correlated patch-clamp FRET anisotropy measurements, cells are subcultured overnight on a 25 mm glass slide in 35 mm petri dish. After subculture, cells are attached on glass slide in petri dish and ready for protein expression when the area of glass slide is covered by 50%. We normally wait for 1−2 day time duration after subculture to start protein expression in live HEK-293 cell by transfecting with plasmid DNA. Plasmid DNA encoding GluN1a and GluN2B are gift from Prof. David R. Lynch, University of Pennsylvania. Plasmids are amplified with a standard method. Amplified plasmids are used for heterogeneous expression in live HEK-293 cell without further purification.[18] In brief, each DNA plasmid of NMDA receptor on Whatman filter paper is separately dissolved in 200 μL of autoclaved and deionized water. Now 10 μL of these plasmids are added to 50 μL of DH5α separately and dipped in ice for 30 min to apply heat-shock followed by sudden change in the temperature to 42 °C for 45 s and then again returning it to ice temperature for 3 min. This method is very crucial to make sure NMDA receptor plasmids are inside of the bacteria. Then we add 1 ml of LB solution to each vial having plasmids with DH5α bacteria and keep them in rotating incubator for 1 hr at 37 °C. An amount of 200 μL of each plasmid solution is added on the surface of previously prepared LB agar plate with antibiotic. Antibiotic is selected according to the structure of plasmid vector and antibiotic resistant gene in it. Each LB plate is kept inside of small incubator for 16 h at a temperature of 37 °C. Bacteria is grown on a LB plate as colony with a copy of NMDA receptor plasmid. Then one of the separate bacterial colony (or dot) is collected and added in 6 mL of LB solution (with no agar) with antibiotic. The solution in a glass test tube is attached in a rotating incubator to grow bacteria for 24 h at 37 °C. In this solution, only those bacteria cells that have NMDA receptor plasmid are grown and that have plasmid that need to be extracted for future preservation. Bacteria are extracted from LB solution by centrifuge and then by making a solution with resuspension reagents (Thermo Scientific, Gene JET Plasmid Miniprep kit, cat. no. K0502). Then we added lysis solution and neutralization solution to separate the cell membranes and plasmids. This solution is collected after centrifuge and filtered through miniprep filter. Finally, we have added 20 μL of hot water twice to collect plasmid solution. The same principle of amplification of plasmid and the extraction is done for each subunit of NMDA receptor DNA plasmid.[18−20,35]

The method of NMDA receptor expression is standard and reported elsewhere.[18,20,32] For efficient gene transfer by transfection, we followed a protocol of lipid-mediated transfection with Lipofectamine LTX and Plus reagent (Invitrogen, 11668-019). The day before transfection, growth media is removed and replaced with growth media without antibiotics (Pen-strep). We mixed GluN1a, GluN2B, and GFP plasmids each 1 μL and 3 μL of Plus reagent in 500 μL of opti-MEM, and then after 5 min, 6 μL of LTX reagent (Invitrogen) was added to the solution. Then the mixture is incubated at room temperature for 25 min. Finally, we added the solution to a petri dish containing HEK-293 cells with a media having no antibiotic. Cells are incubated with 1 μg of cDNA (GluN1a:GluN2B:GFP = 1:1:1) for protein expression in 35 mm petri dish having a 25 mm round-shaped glass slide in it. Cells are also washed with PBS buffer solution before the patch-clamp experiment. GFP is used as a marker of the NMDA receptor expressed in HEK-293 cells for only patch-clamp experiment; whereas, we did not use GFP to avoid fluorescence signal contamination with FRET donor in the correlated experiment.[32] The number of individual cells expressed with NMDA and GFP is examined by fluorescence imaging experiments by an Olympus-IX71 inverted microscope imaging system with a detection system of EMCCD camera.

2.2. Donor and Acceptor Labeling for Simultaneous Single-Molecule FRET and Anisotropy Experiment. NMDA receptor is activated by simultaneous binding of two neurotransmitter molecules: glycine (Gly) and glutamate (Glu) molecule at LBDs of the NMDA receptor ion channel.[2,9,16] Glycine is covalently labeled with Alexa-532 dye followed by multiple HPLC purifications using C8 column with 80% methanol and 1% ACN, which ensures the purity of the dye-labeled glycine. The purity of the labeled molecule is further confirmed by mass spectroscopy. For our single-molecule FRET anisotropy measurements, the Alexa-532-labeled glycine is added in the extracellular solution, which acts as a donor (Figure 1).[32]

After NMDA receptor expression on the HEK-293 cell membrane, an antibody (anti-NMDA receptor-2B covalently attached with ATTO-594, AGC-003-AR) is labeled with GluN2B subunit of the

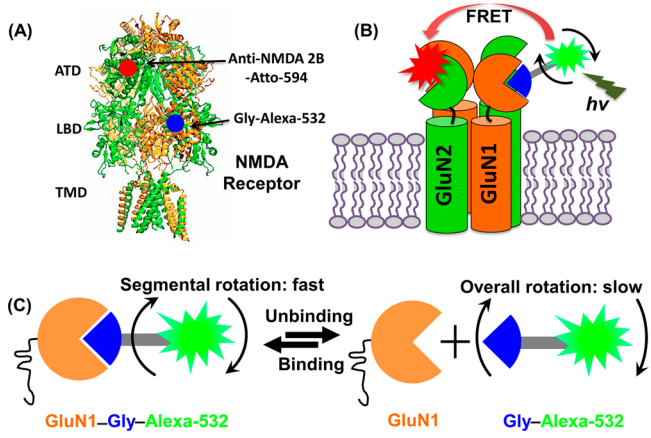

Figure 1. (A) Crystal structure (side view) of NMDA receptor (PDB ID: 4TLL) having four subunits, two are GluN1 (brown) and other two are GluN2B (green). It has three domains: ATD, LBD, and TMD. Position of FRET donor, glycine labeled with Alexa-532 (blue) and acceptor, anti-NMDA receptor 2B labeled with Atto-594 (red) are shown in GluN1 and GluN2B subunits, respectively. (B) Schematic representation of heterotetrameric NMDA receptor ion channel (side view) and single-molecule FRET anisotropy experimental strategy in a live cell. It has two copies of GluN1a subunits (brown) and two copies of GluN2B subunits (green). NMDA receptor ion channel is activated by the binding of glycine and glutamate at the LBD of GluN1 and GluN2, respectively. Agonist ligand glycine is covalently attached with Alexa-532 (green), which acts as donor in the single-molecule FRET experiment. As the donor is free to bind and unbind at the LBD, we can also probe binding events of the ligand by single-molecule anisotropy measurement. GluN2B subunit is labeled with antibody, which is already attached with ATTO-594 (black), acts as acceptor in FRET. (C) Binding and unbinding of glycine, covalently attached with Alexa-532, at the LBD of GluN1 subunit. Binding and unbinding events of ligand are probed by measuring simultaneous single-molecule FRET and anisotropy experiments. At the binding condition, segmental motion of the dye would be observed. However, overall tumbling is observed at the unbinding condition. Segmental motion is much faster than the overall tumbling motion.[36]

DOI: 10.1021/jacs.6b03496
J. Am. Chem. Soc. 2016, 138, 8789−8801

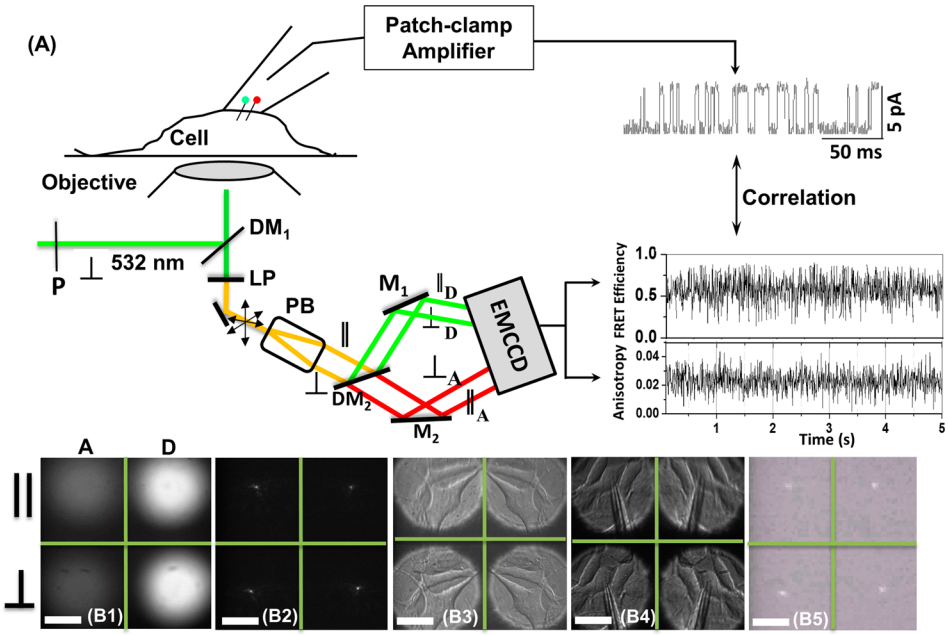

Figure 2. (A) Schematic representation of single-molecule patch-clamp FRET anisotropy microscope setup to study NMDA receptor conformational dynamics and ligand binding kinetics. Single NMDA receptor channel is patched for current measurement. The pipet tip makes the contact with the cell membrane at an incidence angle of 45°. Perpendicularly polarized (P: Polarizer) 532 nm laser excitation is focused through a microscope objective (60×) on the cell. We note that the Alexa-532 labeled glycine ligand is confined in the pipet of 0.5−1 μm tip aperture size. The unpolarized fluorescence signal from donor and acceptor is passed through a 545 nm long-pass filter (LP) and a polarizer beam splitter (PB) to separate out fluorescence to perpendicular (⊥) and parallel (||) polarization. Then a dichroic beam splitter (at 45°) separates signal into two (|| + ⊥) donor channels and two (|| + ⊥) acceptor channels. Four channel fluorescence is recorded by EMCCD camera simultaneously with patch-clamp electric current recording. DM_1: dichroic mirror (Chroma Technology, z532rdc), MD_2: dichroic mirror (Chroma Technology, 645dcxr); LP: 545 nm long-pass filter, M: mirror. Red and green lines are for acceptor and donor fluorescence signal, respectively. The excitation wavelength for the correlated experiment is 532 nm and for antibody labeled cell imaging is 632 nm. (B1) White light splitting in four channel optical setup. (B2) Four channel fluorescence spot recorded with a 1 μm bead. (B3−B4) Four channel DIC imaging of live HEK-293 and at gega-seal condition, respectively. (B5) A frame in correlated fluorescence imaging.

NMDA receptor ion channel (according to protocol, Alomone Lab).[2,9,16] The labeling of the antibody on GluN2B subunit of NMDA receptor ion channel was confirmed by the fluorescence imaging of the live HEK-293 cell by 632 nm laser.[32] To perform correlated patch-clamp and FRET anisotropy measurement, NMDA receptor is expressed without GFP (Altogen Biosystems, cat. no. 4060).[32] As the emission peak of GFP and Alexa-532 are comparatively similar, the presence of GFP may contaminate the fluorescence signal of Alexa-532.

2.3. On-Cell Electrophysiology Experiment: Single-Channel Current Recording. On-cell mode of electrophysiology is used to study single ion channel current fluctuation. To get the best quality data, the experimental stage is kept free from vibration to keep cell-attached patches for long enough to record sufficient data. Activation of NMDA receptor is done by the binding of two neurotransmitter glycine and glutamate. NMDA receptor is also a voltage gated ion channel, and so application of 100 mV is required to start the activation and unblocking of Mg^{2+} ion from the TMD of NMDA receptor. Initially, we start the experiment with a test pulse of 10 mV with 5 ms duration when the pipet is dipped in bath solution. The approach to cell membrane before formation of gega-seal causes the resistance to increase, reducing current by 30%. When the pipet is pushed on the HEK cell, the current becomes slightly smaller to reflect the increasing resistance. Then application of gentle suction increases the resistance further, and within few seconds the resistance becomes in gega-ohm scale. Before starting the data recording, we also verify gega-seal formation by increasing the gain to 50 mV/pA; the trace always appears with very low current except capacitance spikes. Single channel electric currant is recorded with cell-attached patch-clamp technique by applying a fixed voltage as 100 mV through an electrode within the patch-pipet. This pipet is filled with an extracellular solution containing 150 mM NaCl, 2.5 mM KCl, 1 mM EDTA, 10 mM HEPES, pH = 8.0, glucose, 1 mM glutamate, and 0.1 mM glycine or Alexa-532-labeled glycine. Single channel current is recorded without presence of any divalent cations (1 mM EDTA) and at very low concentration of base (pH = 8).

To make a good patch-pipet, borosilicate glass capillary (Sutter Instruments Co., BF150-86-10) is pulled (Sutter Instruments Co., model: P-2000), followed by fire polishing of pipet to reach a high resistance of ∼15−20 MΩ. HEKA EPC-7 Plus amplifier and accusation interface LIH-1600 are used to amplify and record the current, respectively, which is written into digital file with the "Pulse" interfacing software. Off-line data analysis is carried out using PulseFit and Origin 8 software. To maximize the chance of on−off activity from only a single channel, we selected time trajectories of currents, which have no successive opening in current amplitude fluctuation trajectories. No on−off current activity is observed in a control experiment, which is performed without any NMDA receptor ion channel expression in HEK-293 cell.[31] The single-ion channel activity is tested with the ligand, glycine labeled with dye and after antibody binding on the GluN2B subunit of NMDA receptor, and in each case, single-channel current activity is observed.[32] We followed a standard method and protocol for the selection of a cell and the methods of attaching the pipet with motorized micromanipulator on cell membrane.

2.4. Experimental Setup: Correlated Single-Channel Electrophysiology and Single-Molecule Fluorescence Microscopy. Experiment of single-molecule ligand binding at NMDA receptor is performed using a combined setup of single-channel electrophysiology and single-molecule FRET anisotropy four-channel measurement system built in our lab. Figure 2A shows the diagram of our experimental setup. The system is based on an inverted microscope (Olympus IX71) with differential interference contrast (DIC) imaging components. We have previously described the patch-clamp experi-

DOI: 10.1021/jacs.6b03496
J. Am. Chem. Soc. 2016, 138, 8789−8801

ment method.[31] The excitation light from a CW-laser source (λ_{ex} = 532 nm, CrystaLaser) is sent to the total internal reflection fluorescence (TIRF) illumination combiner (model no.: IX2-RFAEVA-2) using a fiber-optics, where a polarizer is set in the path of the beam. Vertically polarized light is passed to the microscope system through the back port of the inverted imaging microscope, which is then reflected by a dichroic beam splitter (Chroma Technology, z532rdc) and focused onto cell membrane by a high numerical-aperture objective (Olympous, UPlanSApo 1.2 NA, 60×). In all correlated patch-clamp and FRET anisotropy experiments, a vertically polarized 532 nm CW-laser is used; however, for antibody-labeled cell imaging, we used a 632 nm He−Ne laser (Figure 2A). The fluorescence image is also recorded through the same objective. The fluorescence signal emitted from the FRET donor (Alexa-532) and acceptor (ATTO-594) is unpolarized. To obtain the fluorescence images and intensity trajectories, the emission signals are passed through a 545 long pass filter. The unpolarized signal of donor−acceptor is then passed through polarizing beam displacer. Beam displacing prisms are used to separate an input beam into two orthogonally polarized output beams and can be used as polarizing beam splitters in applications where the 90° separation of the beams is not possible. The beam displacer made of calcite can provide a beam displacement to 4 mm distance. So after polarizing beam displacer, we have two channels parallel and perpendicular, having the signal mixed with donor and acceptor. A 605 nm dichroic beam splitter at an orientation of 45° angle on the direction of the signal separates out the beam depending on the color of light. A dichroic beam splitter transmits acceptor signal and reflects the donor signal. We then have four channels of signal containing parallel and perpendicular light components for donor and acceptor fluorescence, separately. The donor and acceptor channels are then reflected by two mirrors and focused to an electron multiplying charge-coupled device (EMCCD) camera (Princeton Instruments, ProEM) through two plano-convex lenses for a single-molecule fluorescence signal time-trajectory measurement. Signals are passed through plano-convex lenses on a moving stage to focus properly and cover symmetrically on the 512 × 512 pixel imaging area on EMCCD. A typical raw data of donor channel and acceptor channel are shown in Figure 2B1−B5. The fluorescence signal is recorded in a video having 1000 frames, and each frame has an acquisition time of 5 ms with total acquisition time of 5s. The typical intensity time trajectories of donor and acceptor at two different polarizations are analyzed offline by cross-section intensity analysis at 3 × 3 pixel area on each of 1000 fames.

2.5. Florescence Intensity and Anisotropy Analysis. Fluorescence anisotropy is capable of providing insights into the motions of the probe and orientation. It can be due to either faster subdomain rotation at the binding state or tumbling of entire molecule in solution at the unbinding state. The fluorescence anisotropy $r(t)$ is defined as the difference between the vertically and horizontally polarized fluorescence emission normalized with the total fluorescence emission ($I_{total}(t)$), which is given by

$$I_{total}(t) = I_{\parallel} + 2GI_{\perp} \tag{1}$$

$$r(t) = \frac{I_{\parallel} - GI_{\perp}}{I_{\parallel} + 2GI_{\perp}} \tag{2}$$

where $I_{\parallel}$ and $I_{\perp}$ are the fluorescence intensities of the parallel (∥) and horizontal (⊥) polarized emission components at time t with respect to vertically polarized excitation. For our experiment, G is estimated as 1.8, which is the correct coefficient compensation for the different instrumental detection efficiencies of the various polarized components of the emission. In our experiment, the slow rotation is due to the overall tumbling motion of dye attached with glycine in solution. However, faster rotation is observed due to the segmental motion of dye itself when glycine remains bound to the GluN1 ligand binding pocket.

2.6. Single-Molecule FRET Analysis. Förster resonance energy transfer is a nonradiative process, which is originated by dipole−dipole interaction between the electronic states of donor (D) and acceptor (A) molecules. The process of energy transfer from a donor to an acceptor occurs when the oscillations of an optically-induced electronic coherence of the donor are resonant with the electronic energy gap of the acceptor. Efficiency of energy transfer (E_{FRET}) is sensitive to the interdistance between the donor and acceptor, which is typically in the range of 1−10 nm. The energy transfer efficiency (E_{FRET}) is given by

$$E_{FRET} = \frac{1}{1 + (r/R_0)^6} \tag{3}$$

where r is distance between donor and acceptor molecule, and R_0 is the distance between the donor (D) and acceptor (A) at which energy transfer is equal to 50%. R_0 is defined as the Förster radius and is expressed by the following equation:

$$R_0 = 0.211[\kappa^2 n^{-4} Q_D J(\lambda)]^{1/6} \tag{4}$$

where, n is refractive index of the medium (~1.4 for macromolecules in water), Q_D is the quantum yield of the donor in absence of acceptor, κ^2 is the orientation factor, and $J(\lambda)$ is the spectral overlap between the donor emission and the acceptor absorption. $J(\lambda)$ is related to the normalized fluorescence intensity (I_D) of the donor in the absence of the acceptor and the extinction coefficient of the acceptor (ε_A) as follows:

$$J(\lambda) = \frac{\int_0^\infty I_D(\lambda)\varepsilon_A(\lambda)\lambda^4 d\lambda}{\int_0^\infty I_D(\lambda) d\lambda} \tag{5}$$

We used $\kappa^2 = 2/3$ (random orientation) for the calculation of R_0.

Although the distance measured by FRET is not necessarily accurate as often being specified as a "spectroscopic ruler", single-molecule FRET is sensitive to probe the dynamics of temporal fluctuation occurs by distance changes, such as the conformational changes of the biomolecules. Any process that effects the FRET rate and efficiency enables us to probe the conformational fluctuation dynamics of biomolecules, e.g., protein and ion channel. In single-molecule FRET measurements, E_{FRET} from donor to acceptor reflects mutual distance changes, which results in the capability of probing conformational dynamics of biomolecules at the single molecular level in real time by tracking E_{FRET} changes. The detection of E_{FRET}, usually by ratio-metric methods, can be generally classified into two classes: intensity-based FRET and lifetime-based FRET. We have used intensity-based FRET efficiency measurement method to understand the dynamics of the NMDA receptor ion channel in live HEK-293 cells.

$$E_{FRET}(t) = \frac{I_A(t)}{I_A(t) + I_D(t) \times \frac{\phi_A \times \eta_A}{\phi_D \times \eta_D}} = \frac{I_A(t)}{I_A(t) + I_D(t)} \tag{6}$$

where I_A is the acceptor fluorescence intensity; I_D is the donor fluorescence intensity; ϕ_A and ϕ_D are the emission quantum yields of acceptor and donor dyes, respectively; and η_A and η_D are the acceptor and donor detection efficiencies, respectively. Here the correction factor $(\phi_A \times \eta_A)/(\phi_D \times \eta_D)$ is ~1 in our experiment conditions. The histogram of distribution of E_{FRET} trajectory gives the average E_{FRET} of single molecule.

2.7. Statistical Analysis of Single-Molecule Intensity Trajectories. We performed simultaneous and correlated measurements of real-time single-molecule FRET anisotropy imaging with a single-channel electric current recording for dissecting the conformational state changes associated with the seemingly two-state on−off electric current activities of the NMDA receptor ion channel.

In our experiment, donor and acceptor intensity is recorded in terms of the polarization. To get the total intensity of donor and acceptor, we have added the fluorescence intensity of parallel polarization and perpendicular polarization following eq 1. Finally, we get two channel donor $\{I_D(t)\}$ and acceptor $\{I_A(t)\}$ intensity trajectories. Typically, single-molecule donor−acceptor fluorescence intensity fluctuation trajectories show anticorrelated intensity fluctua-

DOI: 10.1021/jacs.6b03496
J. Am. Chem. Soc. 2016, 138, 8789−8801

tion resulting from intramolecular FRET. Multiple approaches have been performed for the correlation function analysis, including second-order autocorrelation function and cross-correlation function calculated from the donor $\{I_D(t)\}$ and acceptor $\{I_A(t)\}$ fluctuation trajectories.[86] The correlation time between $\{I_D(t)\}$ and $\{I_A(t)\}$ is calculated by autocorrelation function $C_{auto}(t)$ and cross-correlation function $C_{cross}(t)$:

$$C_{cross}(t) = \frac{\langle \Delta I_A(0) \Delta I_D(t) \rangle}{\langle \Delta I_A(0) \Delta I_D(0) \rangle} \quad (7)$$

$$= \frac{\langle (I_A(0) - \langle I_A \rangle)(I_D(t) - \langle I_D \rangle) \rangle}{\langle (I_A(0) - \langle I_A \rangle)(I_D(0) - \langle I_D \rangle) \rangle} \quad (8)$$

When $I_A(t) = I_D(t)$, we have the autocorrelation function:

$$C_{auto}(t) = \frac{\langle \Delta I_A(0) \Delta I_A(t) \rangle}{\langle \Delta I_A(0)^2 \rangle} \quad (9)$$

$$= \frac{\langle (I_A(0) - \langle I_A \rangle)(I_A(t) - \langle I_A \rangle) \rangle}{\langle (I_A(0) - \langle I_A \rangle)^2 \rangle} \quad (10)$$

where $I_A(t)$ and $I_D(t)$ represents the signal variables measured in time trajectories $\{I_A(t)\}$ and $\{I_D(t)\}$. $\langle I_A \rangle$ and $\langle I_D \rangle$ are the means of the fluctuation trajectories of $\{I_A(t)\}$ and $\{I_D(t)\}$, respectively. In our experiment, $\{I_A(t)\}$ and $\{I_D(t)\}$ are the time trajectories of fluorescence photon counts or intensities.

2.8. Computational Modeling. Molecular docking was carried out using Autodock Tools 4.2 for predicting the binding modes and energies of ligand binding to protein.[87,88] Here we docked glycine and glycine labeled with Alexa-532 into the 3D structure of GluN1a subunit (PDB ID: 1PB7), separately. To prepare PDB files of glycine and glycine labeled with Alexa-532, we used Chemdraw and Chem3D software to draw the structures and energy minimization, respectively. Input files for docking are prepared using Gasteiger partial charge calculation method for both protein and ligand. Autodock tools are used to merge nonpolar hydrogens of protein and assign atomic charges. Also the nonpolar hydrogens of ligand were merged, and rotatable bonds were assigned. Auto Grid is used to generate Grid maps for each atom type. These are some Autodock parameters, which are used for the molecular docking of our system numbers of conformer for each molecule are 10 (genetic algorithm, GA runs), GA population size is 150, maximum numbers of energy evaluations are 250,000. Finally, Lamarckian genetic algorithm is used for autodock to search the optimum energy, modes, and binding site for the ligand to the protein. From the output, we have used the conformer for further analysis, which has a maximum number of population with the lowest binding energy.

3. RESULTS AND DISCUSSION

The correlated measurement method of four-channel optical imaging and patch-clamp electric recording simultaneously is capable of characterizing the conformation dynamics of ion channel as well as ligand binding and unbinding dynamics at the LBD of NMDA receptor ion channel, which is never possible either by single-channel patch-clamp current recording or a single-molecule fluorescence imaging technique. In a four-channel optical measurement, unpolarized fluorescence signals are separated out as perpendicular and parallel polarization signal components, and then each polarized component is separated out again to donor and acceptor channels (Figure 2). Typically, the total fluorescence of donor and acceptor is calculated by adding the parallel and perpendicular fluorescence intensity (eq 1). For this study, GluN2B subunit of the NMDA receptor is labeled by antibody that is covalently attached with ATTO-594, which acts as the FRET acceptor in the single-molecule patch-clamp FRET imaging experiments. The agonist ligand, glycine, is covalently labeled with Alexa-532 and acts as the FRET donor (Figure 1). Previously, we have reported that NMDA receptor ion channel remains in an electrically off state when the ligand glycine molecule is bound to LBD using a single-molecule patch-clamp FRET microscopy approach.[31] This conformation is an intermediate closed state when the distance change between two LBDs is ∼7 Å, and the conformation is similar to an open state.[32] However, the agonist remains bound to the LBD. This conformation state is also called as desensitized state.[35] Ligands remain in the solution at the closed state of ion-channel. Therefore, the overall rotation of glycine-Alexa-532 in solution is predicted to be slower than the local rotation of only Alexa-532 part of glycine-Alexa-532 in the open or desensitized state, where the ligand remain bound to LBD. The anisotropy calculation gives us the binding and unbinding state of glycine at the LBD of GluN1 subunit of NMDA receptor. Here, we have demonstrated a new technical approach, single-molecule patch-clamp FRET anisotropy imaging to get correlation of electrically on and off states, optically determined conformational closed and open states by FRET, and binding−unbinding states of glycine ligand by anisotropy measurement at the LBD of GluN1 subunit in live HEK-293 cells.

Figure 2A shows the experimental technique to probe the single NMDA receptor ion channel by simultaneous single-molecule FRET anisotropy imaging and patch-clamp electric recording measurements. A single NMDA receptor ion channel on the HEK-293 cell membrane is patched by on-cell method (Figure 2A). The laser focus point and pipet tip are in an upper-under configuration with the HEK-293 cell at the same measurement point. The rapid decay of laser intensity at the patch-pipet of an incidence angle of ∼45° with the imaging plane can provide a smaller than a femtoliter observation volume. This makes a feasible condition for single-molecule imaging on HEK cell membrane. Extracellular solution containing glutamate and glycine labeled with Alexa-532 are introduced to NMDA receptor through the patch-pipet for correlated experiments. Vertically polarized 532 nm CW-laser is focused by 60× objective onto the cell membrane that is patched with a pipet. The unpolarized fluorescence signals from the donor and acceptor are separated out by a polarizer beamsplitter (PB). Then a dichroic mirror splits the signal depending on the wavelength. A total of four channels are focused on a donor−acceptor four-channel imaging EMCCD camera (Figures 2). Electric current trajectories are recorded by on-cell patch-clamp electric recording method simultaneously with the fluorescence imaging. Hence, the correlation of optical signal and electrical signal identifies the presence of optically intermediate closed state or desensitized state as well as the binding and unbinding state of ligand at the LBD of NMDA receptor. The patch-clamp recording of the electric current flow through a single ion channel over time is the direct measurement of its activity, and these electric current trajectories are classifiable between two well-defined levels. The recording of electric current flow for a single NMDA receptor ion channel is shown in Figure 3A, which clearly shows two levels of electric current amplitudes of ion channel. The current amplitude histogram from Figure 3B shows clearly two states: fully on and fully off with current amplitudes of ∼5 pA and 0 pA, respectively. The histogram of on dwell time (Figure 3D) components is deduced from the trajectory in Figure 3A, showing three time components of 0.45 ms (75%), 7 ms (20%), and 323 ms (10%), respectively. Similarly, the off dwell time histogram gives the time components of 0.5 ms

DOI: 10.1021/jacs.6b03496
J. Am. Chem. Soc. 2016, 138, 8789−8801

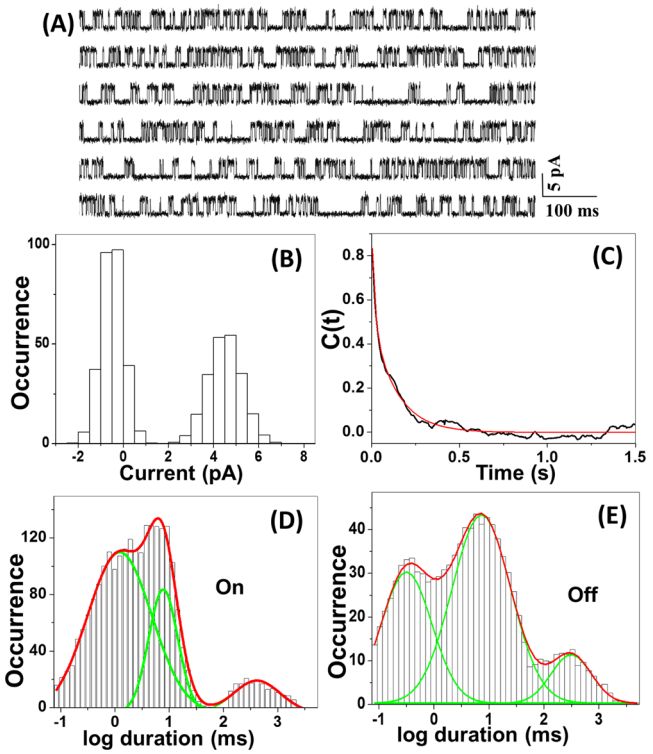

Figure 3. Single-channel current analysis in correlated single-molecule patch-clamp FRET anisotropy microscopy. (A) A typical ion channel current trajectory for single NMDA receptor ion channel recorded in live HEK-293 cell. (B) Distribution of current amplitude, derived from the single-channel current trace in (A), showing two peaks at 0 and 5 pA, which correspond to fully closed state and fully open state of the ion channel, respectively. (C) Decay of autocorrelation function, calculated from the current trajectory in (A). It was best fitted by a two exponential fitting equations with the decay rate constants as, k_{fast} = 81 ± 2 s^{-1} and k_{slow} = 1.3 ± 0.002 s^{-1}. Distribution of (D) on time components and (E) off time components of NMDA receptor ion channel calculated from the current trajectory in (A). The red line is for overall distribution, and the green line is for individual time components. The on dwell time histogram gives three time components of t_1 = 0.45 ms (70%), t_2 = 7 ms (20%), and t_3 = 323 ms (10%). The time components for off dwell time histogram are observed as t_1 = 0.5 ms (30%), t_2 = 9.5 ms (60%) and 310 ms (10%).

(30%), 9.5 ms (60%), and 310 ms (10%) (Figure 3E). We also have performed a control experiment to further confirm that the current trajectories measured are originated from individual NMDA ion channels, showing similar results as our previous publication. Control experiments performed on the HEK-293 cell without NMDA receptor ion-channel expression show no observed current signals beyond the background noises. The decay of autocorrelation function, $C(t)$ (Figure 3C), is deduced from the current trace in Figure 3A using eq 9. Biexponential fitting gives a fast rate constant of 81 ± 2 s^{-1} and a slow rate constant of 1.3 ± 0.002 s^{-1}. It is reported that receptors that have prolonged gating time from miliseconds to minutes can switch their gating modes. It is also reported previously that for NMDA receptor there are three types of open time components: low (<1 ms), medium (1−10 ms), and high (>10 ms) using different types of GluN2 receptors (GluN2A, GluN2B, and GluN2C).[18] The shortest open time component is always similar for all three receptor. However, the longer time component can differ considerably among receptor subunits. Their time trace analysis does not indicate how long individual modes last, or how many times they are visited during the transition, but can quickly indicate how many and which kinds of modes are adopted. Thus, two open time components indicate one mode throughout, three open components indicate that the channel switches behavior at least once, and a record with four open components would most probably contain all three modes. Our results show three time components, which are similar to the previously reported results.[18−20,35] Thus, we can also attribute that the NMDA receptor ion channel in our case changes the conformation in open state at least once. We have also analyzed NMDA receptor conformational fluctuation trajectories simultaneously measured with the electric on−off state change trajectories in our correlated single-molecule FRET imaging and patch-clamp electric recording experiments to determine the conformational state changes associated with the seemingly two-state on−off electric current activities. Figure 4A1 shows a typical pair of

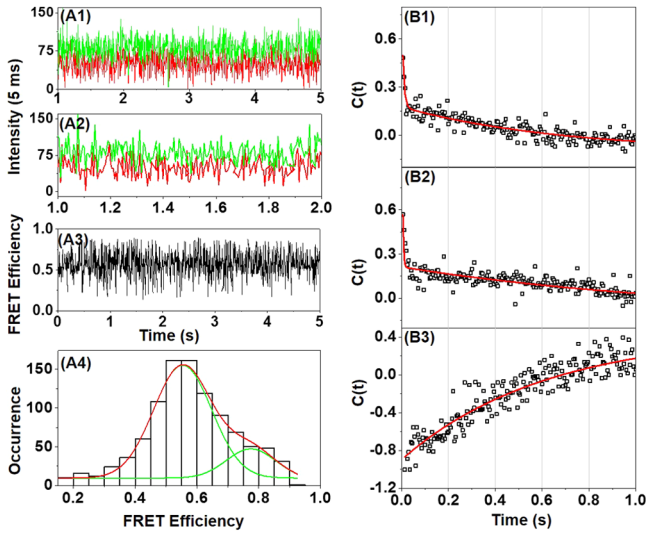

Figure 4. Single-molecule fluorescence intensity fluctuations recording from donor and acceptor of NMDA receptor ion channel in live HEK-293 cell. The total intensity of donor and acceptor is calculated by the equation of $I_{total} = I_{\parallel} + 2GI_{\perp}$. (A1) Typical single-molecule fluorescence intensity fluctuation trajectories with time from donor Alexa-532 (red) and acceptor ATTO-594 (green). (A2) Anticorrelated fluctuation features are evident from the trajectories in zoomed in scale. (A3) FRET efficiency fluctuation trajectory with time and (A4) histogram calculated from the intensity trajectories in panel (A1). Mean FRET efficiency = 0.55 with a range if FRET distribution is from 0.2 to 0.9. (B1) Decay of autocorrelation function of donor. (B2) Decay of autocorrelation function of acceptor. (B3) Decay of cross-correlation function of donor and acceptor. Biexponential fitting gives two decay rate constants, k_{fast} = 65 ± 5 s^{-1} and k_{slow} = 0.45 ± 0.05 s^{-1}.

FRET donor $\{I_D(t)\}$ and acceptor $\{I_A(t)\}$ intensity fluctuation trajectories. The total fluorescence of donor and acceptor is calculated from their intensity at perpendicular and parallel polarization using eq 1. Single-molecule donor−acceptor fluorescence intensity fluctuation trajectories recorded from a single protein molecule are generally anticorrelated intensity fluctuation that results from intramolecular FRET. We have performed second-order autocorrelation function and cross-correlation function analysis calculated from donor−acceptor fluctuation trajectories, $\{I_D(t)\}$ and $\{I_A(t)\}$.[32] The correlation times for $\{I_D(t)\}$ and $\{I_A(t)\}$ are calculated by autocorrelation function $C_{auto}(t)$ and cross-correlation function $C_{cross}(t)$ as per

DOI: 10.1021/jacs.6b03496
J. Am. Chem. Soc. 2016, 138, 8789−8801

eqs 7 and 9, respectively. Here $I_A(t)$ and $I_D(t)$ represent the signal variables measured in time trajectories $\{I_A(t)\}$ and $\{I_D(t)\}$. In our experiment, $\{I_A(t)\}$ and $\{I_D(t)\}$ are the time trajectories of fluorescence photon counts or intensities. Figures 4B1 and 4B2 show typical autocorrelation function analysis of both donor and acceptor fluorescence trajectories, $\langle \Delta I_D(0) \Delta I_D(t) \rangle$ and $\langle \Delta I_A(0) \Delta I_A(t) \rangle$, and the analysis gives essentially the same correlation decay rate constants, a fast decay rate constant of 65 ± 5 s^{-1}, and a slow decay rate constant of 0.45 ± 0.05 s^{-1}. In contrast, the cross-correlation function analysis between the donor and acceptor trajectories, $\langle \Delta I_D(0) \Delta I_A(t) \rangle$, shows anticorrelated results with the same slow decay time as observed in autocorrelation function (Figure 4B3). This strongly indicates that the slow fluctuations of both donor and acceptor fluorescence intensity at a rate of 0.45 ± 0.05 s^{-1} are from the same origin. However, the FRET fluctuation associated with the conformational fluctuations of the NMDA receptor, especially, the conformational changes, are in the coordinates among the four subunits of the ion channel. The identified fast decay rate constant of 65 ± 5 s^{-1} may due to a different source of fluctuation that is nonrelated with the FRET fluctuation and with the associated protein conformational fluctuations based on the fluctuation dissipation theory.[89] Furthermore, the fast component may be due to local fluctuation as the component only shows up in the autocorrelation function but is averaged out in cross-correlation function. The slow fluctuation rate of 0.45 ± 0.05 s^{-1} is originated from the ion channel conformational fluctuation that is relevant to our correlated ion channel dynamics studies. Based on the FRET trajectories, we have also calculated the FRET efficiency histogram, using the eq 6 to evaluate the activity of the ion channels. The mean FRET efficiency is 0.55 (Figure 4A4). The average slow rate constant of electric on−off fluctuation is ∼3 times faster than the average slow rate constant from conformational open−close dynamics. It may be because the electric current measurements can only detect on and off states of ion channel. In case of conformational change, the FRET measurement can identify the intermediate closed states in addition to the open−close conformational states. We have also determined the desensitization state of NMDA receptor ion channel when the ion channel remains in an off state, however, the agonist ligands remain in a binding condition at the LBD. Recently Gouaux and his group reported the structure and dynamics of the GluA2 subunit of the AMPA receptor in the desensitized state by X-ray crystalography.[78] Their studies provide a nearly comprehensive mechanism of full-length AMPA receptor gating and shed new light on the gating mechanism of kainate receptors as well as NMDA receptors. After binding of the agonist at the LBD at the resting state of receptor, one domain tries to close, while the other domain tries to open, resulting separation of each other. This three-dimensional separation exerts an outward pulling force which opens the ion channel. Recently, the distance between the GluN1 and GluN2A subunits within a dimer is measured (72 Å) in the desensitized state of the receptor by FRET, which is longer than the distance in the previously published crystal structure (67 Å) of the isolated LBD of GluN1- GluN2A.[28] Because the dimer interface in the isolated LBD crystallizes in the open channel structure, the longer FRET distances would be consistent with the decoupling of the dimer interface in the desensitized state. This is similar to what has been previously observed for the AMPA subtype of the ionotropic glutamate receptors, suggesting a similar mechanism for desensitization in the two subtypes of the glutamate receptor. Apart from the subunit arrangements, most of the insight into the mechanism of activation, deactivation, and desensitization has been based on the extensive structure−function investigations of the AMPA/NMDA subtype.[9,14,78]

Fluorescence anisotropy is a powerful tool to measure the binding constants and kinetics of the reaction that cause a change in the rotational time of the molecules. If the fluorophore is bound to a small molecule, the rate at which it tumbles can decrease significantly. However, single-molecule anisotropy can also detect the segmental motion or chain motion of the ligand bond to the LBD of ion channel. The degree of binding is also calculated by using the difference in anisotropy of the partially bound, free, and fully bound states measured by titrating the two binding partners. The binding characteristic of the glycine agonist is probed by the single-molecule anisotropy experiment correlated with the electrophysiological experiment. For our experiment, we can predict that the overall rotational motion of glycine bound Alexa-532 in solution (at the unbinding state) would be slower than that of segmental motion of only the Alexa-532 part at the bound state to the LBD of GluN1 subunit. Figure 5A shows an intensity

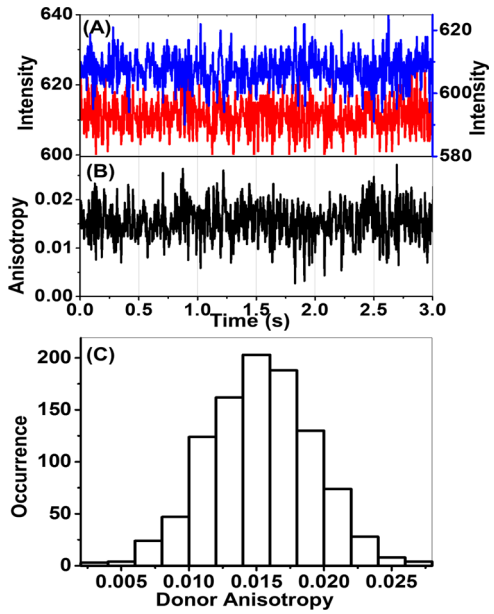

Figure 5. Correlated multiple-parameter spectroscopic measurements of glycine-Alexa-532 binding to NMDA receptor in live HEK-293 cell. (A) Intensity trajectory (5 ms bin) of the parallel polarization component (blue) and perpendicular polarization component (red) for 3 s relative to the excitation polarization in patch-clamp FRET anisotropy microscopy. (B) The lower panel shows single-molecule fluorescence anisotropy fluctuation calculated from the data in upper panel. (C) Anisotropy distribution from the trajectory in (B).

trajectory (5 ms bin) of glycine bound Alexa-532 for the parallel (blue) and perpendicular (red) polarization component with respect to the excitation polarization for 3 s in a correlated patch-clamp FRET anisotropy measurement. Figure 5B shows single-molecule fluorescence anisotropy fluctuation calculated from the data in upper panel. Figure 5C shows the anisotropy distribution of donor from the fluorescence anisotropy trajectory (black) in Figure 5B, which ranges from 0.005 to 0.025 with a peak at around 0.016. Here it is to be noted that the glycine is covalently bound with Alexa-532, thus the

DOI: 10.1021/jacs.6b03496
J. Am. Chem. Soc. 2016, 138, 8789−8801

anisotropy of this system may result from its overall tumbling motion in solution as well as local rotation of Alexa-532 in binding condition at the LBD. To distinguish, a control experiment has been performed to understand rotational behavior of the donor bound to Alexa-532. Figure 6A shows

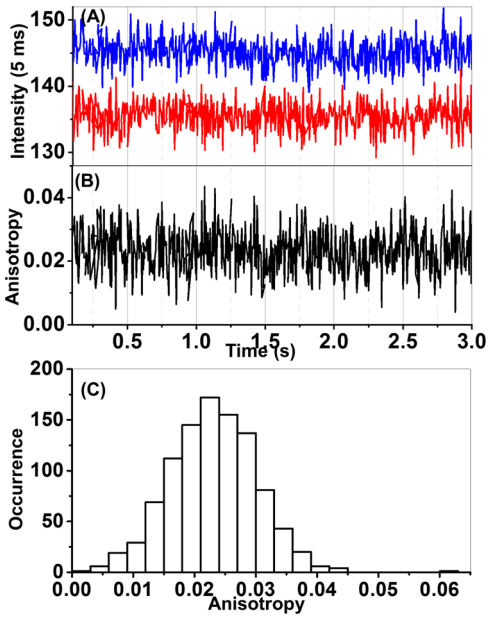

Figure 6. Control optical experimental results of glycine-Alexa-532 in solution only. (A) Intensity trajectory (5 ms bin) of the parallel polarization component (blue) and perpendicular polarization component (red) for 3 s relative to the excitation polarization. This experiment is done in single-molecule patch-clamp FRET anisotropy setup, and data are collected with a 15 nM of glycine-labeled Alexa-532 sample as a control experiment. (B) The lower panel shows single-molecule fluorescence anisotropy fluctuation calculated from the data in upper panel by the eq 2. (C) Anisotropy distribution from the trajectory in (B). The overall distribution of ∼0.02 corresponds to the overall tumbling of glycine covalently attached to Alexa-532 in solution.

the change in anisotropy of glycine covalently labeled with Alexa-532 in only buffer, which is measured by a four-channel optical setup. It is expected that the overall tumbling motion of the glycine covalently bound to Alexa-532 will be slower than the local orientation change of only Alexa-532. It is also well-known that the chain motion or a segmental motion of a protein molecule is much faster than that of overall rotational time in solution.[36] Figure 6C shows a broad distribution of anisotropy ranging from 0.01 to 0.06 with a peak value at 0.022, which clearly indicates that the overall tumbling motion is predominant when the ligand is free to move. However, in the bound state of glycine-Alexa-532 with GluN1 subunit, the local orientation motion of Alexa-532 predominates, which causes a decrease in the overall anisotropy in the correlated experiment. Hence we can say that the anisotropy is a clear signature to probe the binding and unbinding state of ligand with NMDA receptor. Our control experiment shows that single-channel on−off dynamics does not change by changing the agonist ligand glycine to glycine bound to Alexa-532. In addition, the time components for on and off states also remains within the range of reported values (Figure 3). This clearly proves that Alexa-532 does not alter the binding behavior of the glycine at the GluN1 LBD. This is further proved by molecular docking simulation (Figure 7D−F). Dye always remains at the outside of the ligand binding pocket, and an anisotropy measurement typically shows the rotation behavior of the dye even at the bound condition at the GluN1 subunit. As fluorophore is bound to a relatively large GluN1 subunit of NMDA receptor, the change in the mobility accompanying folding can be used to study the dynamics. This provides a measure of the dynamics or kinetics of how the NMDA achieves its conformation transition from open to closed state.

$$R_{NMDA} + L_{Gly} \rightleftarrows R_{NMDA}{:}L_{Gly} \tag{11}$$

At equilibrium,

$$\frac{d[R_{NMDA}{:}L_{Gly}]}{dt} = k_{on}[R_{NMDA}][L_{Gly}] - k_{off}[R_{NMDA}{:}L_{Gly}] \tag{12}$$

and,

$$k_{on}[R_{NMDA}][L_{Gly}] = k_{off}[R_{NMDA}{:}L_{Gly}] \tag{13}$$

$$K_b = \frac{1}{K_d} = \frac{k_{on}}{k_{off}} = \frac{[R_{NMDA}{:}L_{Gly}]}{[R_{NMDA}][L_{Gly}]} = \frac{Ae^{-\Delta G_{on}/RT}}{Ae^{-\Delta G_{off}/RT}} = e^{-\Delta G_b^0/RT} \tag{14}$$

Association and dissociation kinetics as well as binding constant and energy can be calculated using either one of the current data, FRET efficiency, and anisotropy time trajectories. However, the anisotropy time trajectories calculated from correlated experiment are the direct measure of binding and unbinding states of ligand glycine labeled with Alexa-532 to the GluN1 subunit of NMDA receptor. The dwell time histograms for bound and unbound state of glycine-labeled Alexa-532 to GluN1 subunit are deduced from correlated anisotropy data and are shown in Figure 7A,B, respectively. Dwell time histograms are fitted to single exponential decay, and the decay constant is the characteristic time constant of the ligand bound state or unbound state. Dwell time histogram for the bound state (Figure 7A) is defined as the duration of the low level of anisotropy of glycine-Alexa-532, which is best fitted by a single exponential function, yielding a time constant (τ_{bound}) of 8.4 ms that corresponds to the dissociation rate (k_{diss} or k_{off}) of 1.2×10^2 s^{-1}. Similarly, the dwell time histogram for unbound state (Figure 7B) is also fitted with a single exponential function with a time component ($\tau_{unbound}$) of 5.5 ms. The association rate depends on the time constant for unbound state and also the concentration of ligand. For the correlated experiment, the concentration of glycine-labeled Alexa-532 is 0.1 mM, and the association rate (k_{ass} or k_{on}) is calculated as 1.8×10^6 M^{-1} s^{-1}. Now these association and dissociation rate constants are used for measuring the binding constant (K_b) of glycine labeled with Alexa-532 to the GluN1 subunit of NMDA receptor as $K_b = k_{ass}/k_{diss}$ and has been observed as 1.5×10^4 M^{-1}. This value of binding constant is lower than earlier reported values that ranges from 3×10^5 M^{-1} to 10×10^5 M^{-1} for the glycine molecule to NMDA receptor.[90] Recently, Popescu and co-worker have observed the binding constant as 4.2×10^5 M^{-1} with the association and dissociation rate constants of 5×10^6 M^{-1} s^{-1} and 12 s^{-1}, respectively.[35] Here it is to be noted that the dissociation rate constant is the direct measure of time constant for bound state, and we observed it as 1.2×10^2 s^{-1}, which is 10 times higher than the reported value. However, association rate constant value is about 2.8 times lower than the reported one, which indicates that the

DOI: 10.1021/jacs.6b03496
J. Am. Chem. Soc. 2016, 138, 8789−8801

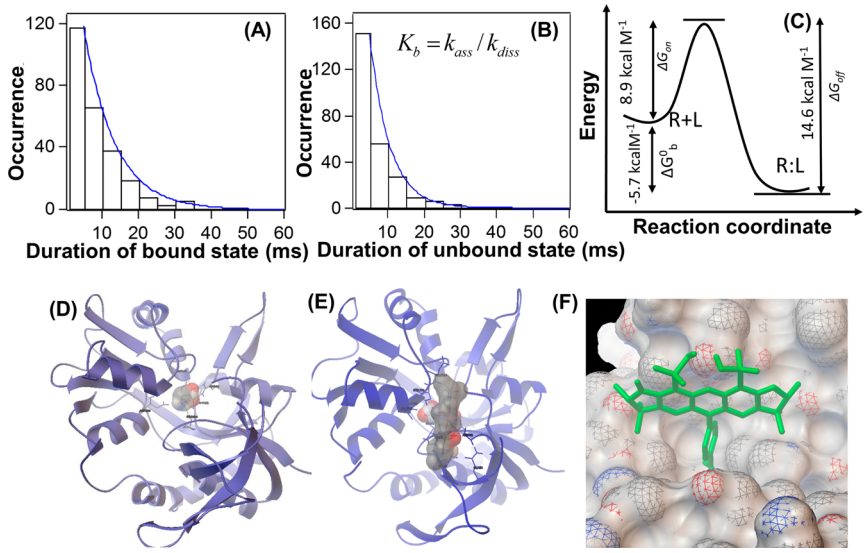

Figure 7. Association and dissociation kinetics between ligand (glycine covalently labeled with Alexa-532) and GluN1 subunit of NMDA receptor ion channel. Dwell time histogram for the bound state (A) and unbound state (B) of glycine-Alexa-532 with GluN1 subunit, which are determined from correlated patch-clamp and anisotropy data as shown in Figure 5B. Each distribution is fitted with a single exponential decay (blue line). (C) A schematic representation for the binding of ligand (glycine labeled with Alexa-532) with GluN1 subunit of NMDA receptor. It depicts that the reaction is proceeding along a reaction coordinate through an activation energy barrier. The overall change in energy is indicated as ΔG^0_b, which is −5.7 kcal M^{-1}, whereas the activation energy for the forward (ΔG_{on}) and backward (ΔG_{off}) reaction of binding are 8.9 kcal M^{-1} and 14.6 kcal M^{-1}, respectively. Docking of ligand glycine (D) and glycine covalently attached with Alexa-532 (E) into the crystal structure (PDB: 1PB7) of GluN1 subunit of NMDA receptor. (F) The crystal structure of GluN1 subunit displayed as molecular surface and atomic sphere, showing the binding cavity where glycine is bound and the Alexa-532 part (green) is outside from the cavity.

contribution of dissociation rate constant is higher for the low value of binding constant. Hence, the lower value of K_b in the current experiment is due to the presence of a bulky group (Alexa-532) on the glycine molecule, which decreases τ_{bound} of glycine to GluN1 subunit of NMDA receptor. These kinetic parameters measured on the single-molecule level for the glycine labeled with Alexa-532 to GluN1 subunit of NMDA receptor are used for further analysis. The free energy of binding has been calculated using the Gibbs free energy equation, $\Delta G^0_b = -RT \ln K_b$, where ΔG^0_b is the free energy of binding and has been observed to be as −5.7 kcal M^{-1}. The free energy of activation for the binding of glycine labeled with Alexa-532 with GluN1 subunit of NMDA receptor was measured using an Arrhenius-like expression from transition-state theory given by Eyring−Polanyi as $k = (k_B T/h)\exp(-\Delta G^{++}/RT)$, where ΔG^{++} is the Gibb's free energy of activation, and k is the rate constant for the reaction. Now using the values of association and dissociation rate constants, the activation energies for the forward and backward reactions for the ligand binding and unbinding are calculated as 8.91 kcal M^{-1} and 14.62 kcal M^{-1}, respectively. These energy representations can be clearly seen in Figure 7C. The difference of activation energies observed from forward and backward rate constant yields free energy of binding, which is exactly same as we observed using Gibb's free energy equation. To validate our findings from the experimental analysis, a computational modeling has also been performed for the blind docking of glycine and glycine labeled with Alexa-532 to GluN1 subunit separately, since we have used glycine-labeled Alexa-532 as a ligand for our experiment, though we have also docked glycine with GluN1 subunit. The reason behind this is to crosscheck the docking results of glycine labeled with Alexa-532, whether it binds to the same site or not and there is any effect of Alexa-532 group in binding. From the docking results we have seen that the glycine binds to the ligand-binding site of GluN1 subunit with an inhibition constant of 27.9 μM, and estimated free energy of binding has been observed as −6.2 kcal M^{-1}. Similarly we have observed that the glycine labeled with Alexa-532 also binds to the ligand-binding site with an inhibition constant of 460 μM, and the free energy of binding has observed as −4.5 kcal M^{-1}; these values are very close to our experimental values. Here it is to be noted that the torsional free energy, which depends on the number of rotational bonds present in the ligand, is higher for glycine labeled with Alexa-532 than only glycine and is additive to the binding free energy that we observed from docking. So the observed binding energy is lower for glycine labeled with Alexa-532 than only glycine. We have further explored the correlated relationship between the simultaneously recorded time trajectories from both electric recording and the FRET anisotropy imaging to identify the correlation between them and to find out intermediate states (Figure 8).

As the recording of the electrical on−off trajectories along with optical signal time-trajectories are done in real time, we can find out relationship between two dynamic signals and determine the intermediates. It is clearly evident that the anisotropy changes from 0.01 to 0.025 at the closed state. The control experiment suggests that the anisotropy of free ligands in solution is ∼0.02. So we can expect a certain extent of the dye to remain in the unbound state in the correlated experiment because of nonspecific binding. However, a subset of anisotropy around 0.01 was also observed, which clearly suggests that there is a certain portion of glycine bound Alexa-532 is either partially or fully bound to the LBD and the ion channel remains at the electrically off state. Gouaux and his co-workers have reported recently the structure and conformation of open, closed, and desensitized states by electron microscopy.[78] They have also shown how agonist binding

DOI: 10.1021/jacs.6b03496
J. Am. Chem. Soc. 2016, 138, 8789−8801

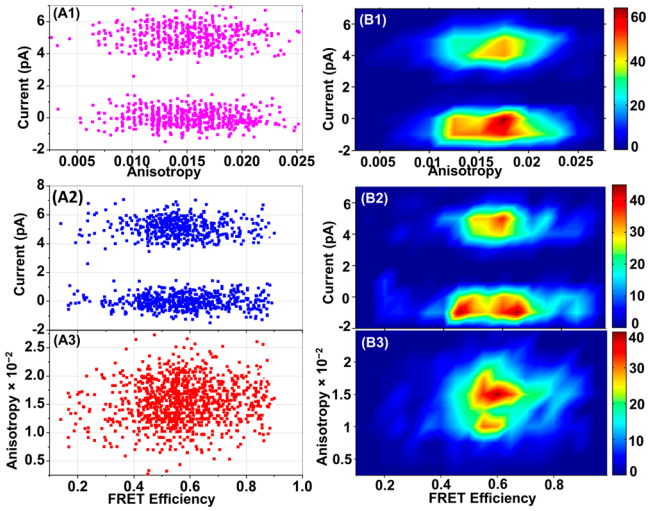

Figure 8. Correlation of single-molecule FRET efficiency, single-molecule anisotropy, and single-channel current amplitude. Typical distribution of raw data is shown in left column, and the right column shows the point density plot. (A1−B1) Distribution of anisotropy with current amplitude. It is evident that the anisotropy distribution is much higher in closed state than the open state. (A2−B2) Distribution of FRET efficiency with current amplitude of NMDA receptor ion channel. Low FRET efficiency is observed for fully on states, whereas high FRET efficiency is observed for fully off states of ion channel. In addition to these fully on−off states, multiple intermediate off states have also been observed that show low FRET efficiency. (A3−B3) Distribution of FRET efficiency and anisotropy. The density plot clearly shows that there are two kinds of distribution of anisotropy.

modulates the conformation of the ligand-binding domain receptors, and how, upon desensitization, the receptor undergoes a significant conformational rearrangements of the amino-terminal and ligand-binding domains. In response to the agonists binding, AMPA receptors ligand-binding dimer interface goes through an outward conformational separation, which exerts a pulling force and goes through a transition state or desensitized state. This crystallographic study also shed new light on the conformational transition of NMDA receptor during activation. It has also been reported how agonists, partial agonists, and antagonists introduced to the GluN1 subunit of NMDA receptor modulate the conformation and activity of the NMDA receptor. The binding of full agonists simply shifts the equilibrium from closed state to open state. Whereas a partial agonist destabilizes an open state and continuously shifts the equilibrium. In the case of AMPA receptor, it also has been shown that the LBD constantly adopts different conformational states depending on the stereochemical properties of the ligand.[13] So from the reported literature, we can speculate that a glycine bound to Alexa-532 ligand may be adopted as a partial agonist in case of activation. This is also supported by the correlation of FRET efficiency and the anisotropy. For single conformation, the anisotropy value changes from 0.01 to 0.02. As this is a dynamic process, the partial rotation may be different because of the effort to adopt a different conformation of LBD in the presence of partial agonists. FRET and current amplitude correlation reconfirm our earlier finding of the existence of the intermediate closed state at the FRET efficiency value of 0.45 (Figure 8A2,B2).

We have proposed a mechanism for open−close transition and ligand binding−unbinding state of NMDA receptor ion channel based on the clamshell type of model for conformation change (Figure 9).[91,92] Our previous report identified the existence of the electrical off state as a subset of intermediate

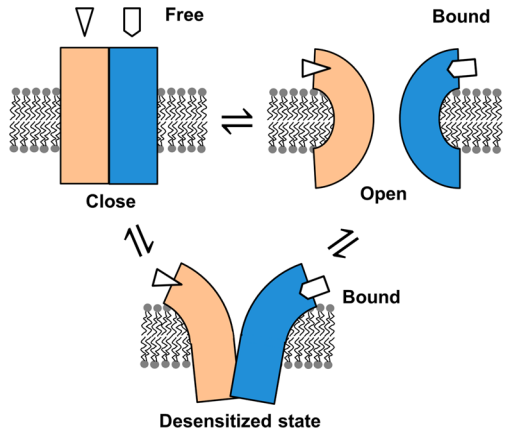

Figure 9. Proposed multistate model of NMDA receptor ion channel open−closed dynamics. It shows the presence of nonconducting or partially conducting ion channel conformation where donor and acceptor are largely separated. At this intermediate closed state, the agonist ligands (glycine and glutamate) are still at the bound condition, which is also called the desensitized state. Desensitization can occur in either open or closed state.

states, which is conformationally similar to the open state of the ion channel. In this work, based on the anisotropy and electrical current amplitude correlation, we have further identified a similar intermediate state, which is an electrically off state. However, at this state, the ligands remain bound at the ligand binding pocket of NMDA receptor during the equilibrium or gating activity. The binding and unbinding activities are determined by the correlation of single-molecule anisotropy and single-channel current amplitude. Experimentally, the desensitized states are detected by correlating the current amplitude fluctuations and anisotropy fluctuation, which occurs due to binding and unbinding of glycine. It is well-known that NMDA receptor exhibits slow response to the presence of agonists, and thus entry to the desensitized state is important to the overall time course of receptor's response. The difficulty in identifying the desensitized state is that both the off state and desensitized state show no flow of ion in the patch-clamp measurement, essentially not resolvable by conventional single ion channel electrophysiological approaches. However, our correlated measurement can directly identify their presence. We assume that desensitization can occur from both open and closed states; although, previous report suggests that desensitization rate is much faster from the open state than from the closed state.[93] Presumably, there could be broadly two different types of desensitized states: one type helps to close the channel, and other type helps to open the channel. The broadness in the correlated data as shown in Figure 8 might be due to the presence of multiple types of desensitized states fluctuating and interexchanging at equilibrium among them. In this case, there will be two possibilities: the first one is that the channel may not enter the fully open state, and the equilibrium is only between the close and the desensitized state. The other possibility is that the equilibrium only occurs between open and desensitized states without entering the fully closed state. According to our proposed model, desensitization can either occur from the open state or closed state. The single-channel patch-clamp electric recording alone cannot distinguish

DOI: 10.1021/jacs.6b03496
J. Am. Chem. Soc. 2016, 138, 8789−8801

between these two type of equilibrium. Nevertheless, correlated patch-clamp and single-molecule FRET anisotropy can detect the presence of multiple states as well as multiple state fluctuations at equilibrium. Furthermore, we have provided evidence that pathways leading to the desensitized state are complex, dynamic, and multistate processes.

4. CONCLUSIONS

In summary, we have developed and demonstrated a new technical method, the single-molecule patch-clamp FRET anisotropy microscopy. This correlated method is capable of simultaneously recording single-molecule FRET efficiency time trajectories associated with conformation changes of single NMDA receptor ions and ligand binding events, i.e., glycine binding at the LBD of the NMDA receptor ion channel by single-molecule anisotropy imaging and patch-clamp single ion channel current trajectories due to the conformational on and off transition. The binding kinetics determined by experiment is further supported by computational modeling. Single-molecule control experiment shows only one kind rotational motion, which is overall tumbling of the ligand. However, in a correlated experiment, we can probe the binding state and unbinding state of ligand by distinguishing the overall anisotropy and the anisotropy of the probe molecule at the binding state at the LBD. Correlating the optical imaging and electrophysiological recording of single ion channel NMDA receptor in live HEK-293 cells simultaneously also suggests the existence of multiple conformation states during the open−close activity of the NMDA receptor ion channel, although the complex conformational dynamics gives apparently simple on−off two-state electric change dynamics. Moreover, the electric on and off state transition goes through a transition state (desensitized state) where agonists remain bound to the ligand binding cleft. The desensitized state can occur from either open state or closed state. Furthermore, this observation reconfirmed our previous observation of existing multiple intermediate conformational states, which have similar conformations as that of the open state, however they are electrically off state. Technically, the demonstrated method can probe simultaneously the agonist binding kinetics as well as ion channel conformation dynamics.

AUTHOR INFORMATION

Corresponding Author

*hplu@bgsu.edu

Notes

The authors declare no competing financial interest.

ACKNOWLEDGMENTS

We thank Prof. Anthony L. Auerbach, Department of Physiology and Biophysics, State University of New York, Buffalo, NY for sending us HEK-293 cell as a gift. We also acknowledge Prof. David R. Lynch, University of Pennsylvania for providing us DNA plasmids of NMDA receptor. This work is supported by NIH/NIGMS and the Ohio Eminent Scholar Endowment.

REFERENCES

(1) Li, F.; Tsien, J. Z. *N. Engl. J. Med.* **2009**, *361* (3), 302.
(2) Traynelis, S. F.; Wollmuth, L. P.; McBain, C. J.; Menniti, F. S.; Vance, K. M.; Ogden, K. K.; Hansen, K. B.; Yuan, H.; Myers, S. J.; Dingledine, R. *Pharmacol. Rev.* **2010**, *62* (3), 405.
(3) Vance, K. M.; Simorowski, N.; Traynelis, S. F.; Furukawa, H. *Nat. Commun.* **2011**, *2*, 294.
(4) Yuan, H.; Myers, S. J.; Wells, G.; Nicholson, K. L.; Swanger, S. A.; Lyuboslavsky, P.; Tahirovic, Y. A.; Menaldino, D. S.; Ganesh, T.; Wilson, L. J.; Liotta, D. C.; Snyder, J. P.; Traynelis, S. F. *Neuron* **2015**, *85* (6), 1305.
(5) Hansen, K. B.; Ogden, K. K.; Yuan, H.; Traynelis, S. F. *Neuron* **2014**, *81* (5), 1084.
(6) Erreger, K.; Geballe, M. T.; Dravid, S. M.; Snyder, J. P.; Wyllie, D. J. A.; Traynelis, S. F. *J. Neurosci.* **2005**, *25* (34), 7858.
(7) Banke, T. G.; Traynelis, S. F. *Nat. Neurosci.* **2003**, *6* (2), 144.
(8) Hansen, K. B.; Burger, P.; Vance, K. M.; Snyder, J. P.; Clausen, R. P.; Traynelis, S. F. *Biophys. J.* **2010**, *98* (3), 525a.
(9) Lee, C.-H.; Lü, W.; Michel, J. C.; Goehring, A.; Du, J.; Song, X.; Gouaux, E. *Nature* **2014**, *511* (7508), 191.
(10) Lee, C.-H.; Gouaux, E. *PLoS One* **2011**, *6* (4), e19180.
(11) Sobolevsky, A. I.; Rosconi, M. P.; Gouaux, E. *Nature* **2009**, *462* (7274), 745.
(12) Jin, R.; Singh, S. K.; Gu, S.; Furukawa, H.; Sobolevsky, A. I.; Zhou, J.; Jin, Y.; Gouaux, E. *EMBO J.* **2009**, *28* (12), 1812.
(13) Inanobe, A.; Furukawa, H.; Gouaux, E. *Neuron* **2005**, *47* (1), 71.
(14) Furukawa, H.; Singh, S. K.; Mancusso, R.; Gouaux, E. *Nature* **2005**, *438* (7065), 185.
(15) Furukawa, H.; Gouaux, E. *EMBO J.* **2003**, *22* (12), 2873.
(16) Karakas, E.; Furukawa, H. *Science* **2014**, *344* (6187), 992.
(17) Jespersen, A.; Tajima, N.; Fernandez-Cuervo, G.; Garnier-Amblard, E. C.; Furukawa, H. *Neuron* **2014**, *81* (2), 366.
(18) Amico-Ruvio, S. A.; Popescu, G. K. *Biophys. J.* **2010**, *98* (7), 1160.
(19) Popescu, G. K. *J. Physiol.* **2012**, *590*, 73.
(20) Zhang, W.; Howe, J. R.; Popescu, G. K. *Nat. Neurosci.* **2008**, *11* (12), 1373.
(21) Das, U.; Kumar, J.; Mayer, M. L.; Plested, A. J. R. *Proc. Natl. Acad. Sci. U. S. A.* **2010**, *107* (18), 8463.
(22) Lipton, S. A. *Nat. Neurosci.* **2008**, *11* (4), 381.
(23) Piña-Crespo, J. C.; Talantova, M.; Micu, I.; States, B.; Chen, H.-S. V.; Tu, S.; Nakanishi, N.; Tong, G.; Zhang, D.; Heinemann, S. F.; Zamponi, G. W.; Stys, P. K.; Lipton, S. A. *J. Neurosci.* **2010**, *30* (34), 11501.
(24) Dai, J.; Zhou, H. X. *Biophys. J.* **2013**, *104* (10), 2170.
(25) Yao, Y.; Belcher, J.; Berger, A. J.; Mayer, M. L.; Lau, A. Y. *Structure* **2013**, *21* (10), 1788.
(26) MacDermott, A. B.; Mayer, M. L.; Westbrook, G. L.; Smith, S. J.; Barker, J. L. *Nature* **1986**, *321* (6069), 519.
(27) Foucaud, B.; Laube, B.; Schemm, R.; Kreimeyer, A.; Goeldner, M.; Betz, H. *J. Biol. Chem.* **2003**, *278* (26), 24011.
(28) Rambhadran, A.; Gonzalez, J.; Jayaraman, V. *J. Biol. Chem.* **2010**, *285* (20), 15296.
(29) Sobczyk, A.; Scheuss, V.; Svoboda, K. *J. Neurosci.* **2005**, *25*, 6037.
(30) Mayer, M. L. *Structure* **2011**, *19* (10), 1370.
(31) Dai, J.; Wollmuth, L.; Zhou, H.-X. *J. Phys. Chem. B* **2015**, *119* (34), 10934.
(32) Sasmal, D. K.; Lu, H. P. *J. Am. Chem. Soc.* **2014**, *136* (37), 12998.
(33) Sobolevsky, A. I.; Prodromou, M. L.; Yelshansky, M. V.; Wollmuth, L. P. *J. Gen. Physiol.* **2007**, *129* (6), 509.
(34) Mayer, M. L. *Nature* **2006**, *440* (7083), 456.
(35) Cummings, K. A.; Popescu, G. K. *J. Gen. Physiol.* **2015**, *145* (6), 513.
(36) Nicastro, G.; Margiocco, P.; Cardinali, B.; Stagnaro, P.; Cauglia, F.; Cuniberti, C.; Collini, M.; Thomas, D.; Pastore, A.; Rocco, M. *Biophys. J.* **2004**, *87* (2), 1227.
(37) Weatherill, E. E.; Wallace, M. I. *J. Mol. Biol.* **2015**, *427* (1), 146.
(38) Wang, Y.; Liu, Y.; Deberg, H. A.; Nomura, T.; Hoffman, M. T.; Rohde, P. R.; Schulten, K.; Martinac, B.; Selvin, P. R. *eLife* **2014**, *3*, e01834.
(39) Song, W.; Pang, P.; He, J.; Lindsay, S. *ACS Nano* **2013**, *7* (1), 689.

DOI: 10.1021/jacs.6b03496
J. Am. Chem. Soc. 2016, 138, 8789−8801

(40) Kong, L.; Harrington, L.; Li, Q.; Cheley, S.; Davis, B. G.; Bayley, H. *Nat. Chem.* **2013**, *5*, 651.
(41) Miranda, P.; Contreras, J. E.; Plested, A. J. R.; Sigworth, F. J.; Holmgren, M.; Giraldez, T. *Proc. Natl. Acad. Sci. U. S. A.* **2013**, *110* (13), 5217.
(42) Rajapaksha, S. P.; Wang, X.; Lu, H. P. *Anal. Chem.* **2013**, *85* (19), 8951.
(43) Bartsch, P.; Walter, C.; Selenschik, P.; Honigmann, A.; Wagner, R. *Materials* **2012**, *5* (12), 2705.
(44) Castell, O. K.; Berridge, J.; Wallace, M. I. *Angew. Chem., Int. Ed.* **2012**, *51* (13), 3134.
(45) Schmauder, R.; Kosanic, D.; Hovius, R.; Vogel, H. *ChemBioChem* **2011**, *12* (16), 2431.
(46) Leptihn, S.; Thompson, J. R.; Ellory, J. C.; Tucker, S. J.; Wallace, M. I. *J. Am. Chem. Soc.* **2011**, *133* (24), 9370.
(47) Hall, L. T.; Hill, C. D.; Cole, J. H.; Städler, B.; Caruso, F.; Mulvaney, P.; Wrachtrup, J.; Hollenberg, L. C. L. *Proc. Natl. Acad. Sci. U. S. A.* **2010**, *107* (44), 18777.
(48) Ide, T. *ChemPhysChem* **2010**, *11* (16), 3408.
(49) Zhao, Y.; Terry, D.; Shi, L.; Weinstein, H.; Blanchard, S. C.; Javitch, J. A. *Nature* **2010**, *465* (7295), 188.
(50) Nakajo, K.; Ulbrich, M. H.; Kubo, Y.; Isacoff, E. Y. *Proc. Natl. Acad. Sci. U. S. A.* **2010**, *107* (44), 18862.
(51) Heron, A. J.; Thompson, J. R.; Cronin, B.; Bayley, H.; Wallace, M. I. *J. Am. Chem. Soc.* **2009**, *131* (5), 1652.
(52) Lu, H. P. *Methods Cell Biol.* **2008**, *90*, 435.
(53) Zheng, J. *Physiology* **2006**, *21* (1), 6.
(54) Peng, S.; Publicover, N. G.; Kargacin, G. J.; Duan, D.; Airey, J. A.; Sutko, J. L. *Biophys. J.* **2004**, *86*, 134.
(55) Chandler, E. L.; Smith, A. L.; Burden, L. M.; Kasianowicz, J. J.; Burden, D. L. *Langmuir* **2004**, *20* (3), 898.
(56) Harms, G.; Orr, G.; Lu, H. P. *Appl. Phys. Lett.* **2004**, *84* (10), 1792.
(57) Selvin, P. R. *Biophys. J.* **2003**, *84* (1), 1.
(58) Peters, R. *Annu. Rev. Biophys. Biomol. Struct.* **2003**, *32*, 47.
(59) Harms, G. S.; Orr, G.; Montal, M.; Thrall, B. D.; Colson, S. D.; Lu, H. P. *Biophys. J.* **2003**, *85* (3), 1826.
(60) Borisenko, V.; Lougheed, T.; Hesse, J.; Füreder-Kitzmüller, E.; Fertig, N.; Behrends, J. C.; Woolley, G. A.; Schütz, G. J. *Biophys. J.* **2003**, *84* (1), 612.
(61) Ide, T.; Takeuchi, Y.; Yanagida, T. *Single Mol.* **2002**, *3*, 33.
(62) Sonnleitner, A.; Mannuzzu, L. M.; Terakawa, S.; Isacoff, E. Y. *Proc. Natl. Acad. Sci. U. S. A.* **2002**, *99* (20), 12759.
(63) Zou, H.; Lifshitz, L. M.; Tuft, R. A.; Fogarty, K. E.; Singer, J. J. *Proc. Natl. Acad. Sci. U. S. A.* **2002**, *99* (9), 6404.
(64) Lougheed, T.; Borisenko, V.; Hand, C. E.; Woolley, G. A. *Bioconjugate Chem.* **2001**, *12* (4), 594.
(65) Harms, G. S.; Cognet, L.; Lommerse, P. H.; Blab, G. A.; Kahr, H.; Gamsjäger, R.; Spaink, H. P.; Soldatov, N. M.; Romanin, C.; Schmidt, T. *Biophys. J.* **2001**, *81* (5), 2639.
(66) Zheng, J.; Zagotta, W. N. *Neuron* **2000**, *28* (2), 369.
(67) Ide, T.; Yanagida, T. *Biochem. Biophys. Res. Commun.* **1999**, *265* (2), 595.
(68) Veatch, W.; Stryer, L. *J. Mol. Biol.* **1977**, *113* (1), 89.
(69) Lu, Q.; Lu, H. P.; Wang, J. *Phys. Rev. Lett.* **2007**, *98*, 128105.
(70) Wang, Y.; Tang, C.; Wang, E.; Wang, J. *PLoS Comput. Biol.* **2012**, *8* (4), e1002471.
(71) Wang, Y.; Gan, L.; Wang, E.; Wang, J. *J. Chem. Theory Comput.* **2013**, *9* (1), 84.
(72) Wang, Y.; Chu, X.; Longhi, S.; Roche, P.; Han, W.; Wang, E.; Wang, J. *Proc. Natl. Acad. Sci. U. S. A.* **2013**, *110* (40), E3743.
(73) Tsytlonok, M.; Craig, P. O.; Sivertsson, E.; Serquera, D.; Perrett, S.; Best, R. B.; Wolynes, P. G.; Itzhaki, L. S. *Structure* **2013**, *21* (11), 1954.
(74) Li, J.; Jonsson, A. L.; Beuming, T.; Shelley, J. C.; Voth, G. A. *J. Am. Chem. Soc.* **2013**, *135* (23), 8749.
(75) Dryga, A.; Chakrabarty, S.; Vicatos, S.; Warshel, A. *Proc. Natl. Acad. Sci. U. S. A.* **2012**, *109* (9), 3335.
(76) Katira, S.; Mandadapu, K. K.; Vaikuntanathan, S.; Smit, B.; Chandler, D. *eLife* **2016**, *5*, e13150.
(77) Landes, C. F.; Rambhadran, A.; Taylor, J. N.; Salatan, F.; Jayaraman, V. *Nat. Chem. Biol.* **2011**, *7* (3), 168.
(78) Dürr, K. L.; Chen, L.; Stein, R. A.; De Zorzi, R.; Folea, I. M.; Walz, T.; Mchaourab, H. S.; Gouaux, E. *Cell* **2014**, *158* (4), 778.
(79) Cleary, L.; Chen, H.; Chuang, C.; Silbey, R. J.; Cao, J. *Proc. Natl. Acad. Sci. U. S. A.* **2013**, *110* (21), 8537.
(80) Gopich, I. V.; Szabo, A. *Proc. Natl. Acad. Sci. U. S. A.* **2012**, *109* (20), 7747.
(81) Wang, S.; Vafabakhsh, R.; Borschel, W. F.; Ha, T.; Nichols, C. G. *Nat. Struct. Mol. Biol.* **2016**, *23*, 31.
(82) Cai, E.; Ge, P.; Lee, S. H.; Jeyifous, O.; Wang, Y.; Liu, Y.; Wilson, K. M.; Lim, S. J.; Baird, M. A.; Stone, J. E.; Lee, K. Y.; Davidson, M. W.; Chung, H. J.; Schulten, K.; Smith, A. M.; Green, W. N.; Selvin, P. R. *Angew. Chem., Int. Ed.* **2014**, *53* (46), 12484.
(83) Abdelfattah, A. S.; Farhi, S. L.; Zhao, Y.; Brinks, D.; Zou, P.; Ruangkittisakul, A.; Platisa, J.; Pieribone, V. A.; Ballanyi, K.; Cohen, A. E.; Campbell, R. E. *J. Neurosci.* **2016**, *36* (8), 2458.
(84) Dani, A.; Huang, B.; Bergan, J.; Dulac, C.; Zhuang, X. *Neuron* **2010**, *68* (5), 843.
(85) Venkatachalam, V.; Cohen, A. E. *Biophys. J.* **2014**, *107* (7), 1554.
(86) Lu, H. P. *Chem. Soc. Rev.* **2014**, *43* (4), 1118.
(87) Morris, G. M.; Huey, R.; Lindstrom, W.; Sanner, M. F.; Belew, R. K.; Goodsell, D. S.; Olson, A. J. *J. Comput. Chem.* **2009**, *30* (16), 2785.
(88) Morris, G. M.; Goodsell, D. S.; Halliday, R. S.; Huey, R.; Hart, W. E.; Belew, R. K.; Olson, A. J. *J. Comput. Chem.* **1998**, *19* (14), 1639.
(89) Chandler, D.; Percus, J. K. *Introduction to Modern Statistical Mechanics*; Oxford University Press: Oxford, U.K., 1988; Vol. *41*.
(90) Lester, R. A.; Tong, G.; Jahr, C. E. *J. Neurosci.* **1993**, *13* (3), 1088.
(91) Perrais, D.; Veran, J.; Mulle, C. *Trends Pharmacol. Sci.* **2010**, *31* (11), 516.
(92) Chaudhry, C.; Weston, M. C.; Schuck, P.; Rosenmund, C.; Mayer, M. L. *EMBO J.* **2009**, *28* (10), 1518.
(93) Lin, F.; Stevens, C. F. *J. Neurosci.* **1994**, *14* (4), 2153.

DOI: 10.1021/jacs.6b03496
J. Am. Chem. Soc. 2016, 138, 8789−8801